Clin Orthop Relat Res (2019) 477:1053-1063
DOI 10.1097/CORR.0000000000000528

Clinical Orthopaedics and Related Research®
A Publication of The Association of Bone and Joint Surgeons®

2018 Bernese Hip Symposium

Cam FAI and Smaller Neck Angles Increase Subchondral Bone Stresses During Squatting: A Finite Element Analysis

K. C. Geoffrey Ng PhD, Giulia Mantovani PhD, Mario Lamontagne PhD, Michel R. Labrosse PhD, Paul E. Beaulé MD, FRCSC

Received: 31 May 2018 / Accepted: 24 September 2018 / Published online: 27 November 2018

Abstract

Background Individuals with a cam deformity and a decreased (varus) femoral neck-shaft angle may be predisposed to symptomatic femoroacetabular impingement (FAI). However, it is unclear what combined effects the cam deformity and neck angle have on acetabular cartilage and subchondral bone stresses during an impinging squat motion. We therefore used finite element analysis to examine the combined effects of cam morphology and femoral neck-shaft angle on acetabular cartilage and subchondral bone stresses during squatting, examining the differences in stress characteristics between symptomatic and asymptomatic individuals with cam deformities and individuals without cam deformities and no hip pain.

Questions/purposes Using finite element analysis in this population, we asked: (1) What are the differences in acetabular cartilage stresses? (2) What are the differences in subchondral bone stresses? (3) What are the effects of high and low femoral neck-shaft angles on these stresses?

Methods Six male participants were included to represent three groups (symptomatic cam, asymptomatic cam, control without cam deformity) with two participants per group, one with the highest femoral neck-shaft angle and

One or more of the authors (ML, PEB) received funding from the Canadian Institutes of Health Research (97778A). One or more of the authors (ML, MRL) received funding from the Natural Sciences and Engineering Research Council of Canada (106769-2013, RGPIN-2017-04588).
Clinical Orthopaedics and Related Research® neither advocates nor endorses the use of any treatment, drug, or device. Readers are encouraged to always seek additional information, including FDA-approval status, of any drug or device prior to clinical use.
Each author certifies that his or her institution approved the human protocol for this investigation and that all investigations were conducted in conformity with ethical principles of research.
This work was performed at the Human Movement Biomechanics Laboratory, University of Ottawa, and at The Ottawa Hospital, Ottawa, Canada.

K. C. G. Ng, Department of Mechanical Engineering, Imperial College London, London, UK

K. C. G. Ng, G. Mantovani, M. Lamontagne, Human Movement Biomechanics Laboratory, University of Ottawa, Ottawa, Ontario, Canada

G. Mantovani, M. Lamontagne, School of Human Kinetics, University of Ottawa, Ottawa, Ontario, Canada

M. Lamontagne, M. R. Labrosse, Department of Mechanical Engineering, University of Ottawa, Ottawa, Ontario, Canada

M. Lamontagne, P. E. Beaulé, Division of Orthopaedic Surgery, University of Ottawa, Ottawa, Ontario, Canada

P. E. Beaulé (✉), Division of Orthopaedic Surgery, The Ottawa Hospital–General Campus, 501 Smyth Road, CCW 1640, Ottawa, ON, K1H 8L6, Canada, email: pbeaule@toh.ca

All ICMJE Conflict of Interest Forms for authors and *Clinical Orthopaedics and Related Research*® editors and board members are on file with the publication and can be viewed on request.

Wolters Kluwer

one with the lowest (that is, most valgus and most varus neck angles, respectively). Each participant's finite element hip models were reconstructed from imaging data and assigned subject-specific bone material properties. Hip contact forces during squatting were determined and applied to the finite element models to examine maximum shear stresses in the acetabular cartilage and subchondral bone.

Results Both groups with cam deformities experienced higher subchondral bone stresses than cartilage stresses. Both groups with cam deformities also had higher subchondral bone stresses (symptomatic with high and low femoral neck-shaft angle = 14.1 and 15.8 MPa, respectively; asymptomatic with high and low femoral neck-shaft angle = 10.9 and 13.0 MPa, respectively) compared with the control subjects (high and low femoral neck-shaft angle = 6.4 and 6.5 MPa, respectively). The symptomatic and asymptomatic participants with low femoral neck-shaft angles had the highest cartilage and subchondral bone stresses in their respective subgroups. The asymptomatic participant with low femoral neck-shaft angle (123°) demonstrated anterolateral subchondral bone stresses (13.0 MPa), similar to the symptomatic group. The control group also showed no differences between cartilage and subchondral bone stresses.

Conclusions The resultant subchondral bone stresses modeled here coincide with findings that acetabular subchondral bone is denser in hips with cam lesions. Future laboratory studies will expand the parametric finite element analyses, varying these anatomic and subchondral bone stiffness parameters to better understand the contributions to the pathomechanism of FAI.

Clinical Relevance Individuals with a cam deformity and more varus neck orientation may experience elevated subchondral bone stresses, which may increase the risks of early clinical signs and degenerative processes associated with FAI, whereas individuals with cam morphology and normal-to-higher femoral neck-shaft angles may be at lesser risk of disease progression that would potentially require surgical intervention.

Introduction

Femoroacetabular impingement (FAI) is described as a pathomechanical failure process of the hip leading to eventual joint degeneration [17]. It is attributed to an abnormal bone deformity that can be characterized as an enlarged femoral head-neck junction (cam type), severe acetabular overcoverage (pincer type), or a combination of both (mixed type) [16, 17]. Mechanical impingement is commonly experienced at the extremes of hip motion, which can result in elevated hip stresses and precede early cartilage degeneration and osteoarthritis [1, 5]. The cam deformity itself is an enlarged bony prominence over the femoral head-neck junction, characterized as an aspherical femoral head with elevated α angles [47, 51, 60, 62]. Individuals with cam FAI often demonstrate restricted joint motion during walking, stair ascent/descent, and squatting [26, 30, 32, 33, 39, 41, 54, 55] as well as pain attributed to trauma, injuries, or labral tears. Conversely, there is a growing population of individuals with cam deformities who may never experience symptoms for much of their adult life [10, 20, 28, 31], although the concern for these asymptomatic individuals is that they may still be susceptible to subchondral bone stiffening [50, 59] and eventual cartilage degeneration [2, 6, 35]. It has recently been observed that individuals with a cam deformity and a smaller femoral neck angle may be more predisposed to early-onset hip pain [4, 39, 40, 52], although it is unknown what combined effects these parameters (cam deformity and neck angle) have on impingement during hip loading.

In recent years, finite element methods have been used to simulate cam FAI and examine resultant hip stresses [11, 12, 23, 27, 46]. Previous simulations indicated that patients with cam FAI experienced elevated stresses at higher amplitudes of motion (such as with sit to stand, squatting, and deep flexion) in comparison with those with normal hips. However, there was a lack of subject specificity in several of the previous in silico studies, in which many of the studies did not consider subject-specific material properties or loading parameters to adequately represent participant groups nor examine a clinically defined asymptomatic population [42]. Our earlier study compared symptomatic and asymptomatic cam morphologies, examining the instance of peak joint loading during level walking [44]. Although both symptomatic and asymptomatic cam morphologies demonstrated higher stresses than control hips, only marginal differences in stress concentrations were observed between each participant's acetabular cartilage and subchondral bone. This lower subchondral bone stress could have been attributed to the relatively small ROM during walking.

Therefore, the purpose of this study was to use finite element analysis to examine the combined effects of cam morphology and femoral neck-shaft angle on hip stresses during squatting, examining the differences in stress characteristics between symptomatic and asymptomatic patients with cam deformities and individuals with normal hips, by asking: (1) What are the differences in acetabular cartilage stresses? (2) What are the differences in subchondral bone stresses? (3) What are the effects of high and low femoral neck-shaft angles on these stresses?

Patients and Methods

Six male participants (n = 6; age, 32 ± 7 years; body mass index [BMI], 26 ± 3 kg/m^2) from a larger participant

cohort were selected for this study [39, 41, 44]. From the larger cohort, all participants completed pain questionnaires—Hip Disability and Osteoarthritis Outcome Score and WOMAC—to confirm symptoms. The participants who presented with a cam deformity and clinical signs were considered symptomatic, whereas the participants who indicated a cam deformity but showed no clinical signs were considered asymptomatic; and the participants who did not have a cam deformity or clinical signs were considered control subjects. (Aside from the symptomatic participants, the remaining participants were unaware whether they had a cam deformity until after the data acquisition protocol.) As a result, the larger cohort from the earlier study consisted of 12 symptomatic, 17 asymptomatic, and 14 control participants to select from [39]. For the symptomatic, asymptomatic, and control groups, the affected hip for comparison was the hip with clinical signs, larger cam deformity, and smaller cam deformity, respectively.

Each participant was imaged using a conventional CT scanner in a supine position (Acquilion™, Toshiba Medical Systems Corporation, Markham, Ontario, Canada; or Discovery CT750, GE Healthcare, Mississauga, Ontario, Canada), imaging the iliac crest to the proximal diaphysis as well as the femoral condyles (512 × 512 resolution, slice thickness of 0.625 mm, 120 kVp, 200 mAs). A calibration phantom (Model 3; Mindways Software, Austin, TX, USA) was placed under the lumbar vertebra for bone densitometry and the natural lordosis was confirmed with a scout scan. In efforts to minimize skin artifacts and pelvic misalignments during motion capture, radiopaque surface markers were placed onto each participant's left and right anterosuperior iliac spines and posterosuperior iliac spines before CT imaging [34]. The CT data were reviewed by a senior musculoskeletal radiologist (KR) for a cam deformity, indicated by either an axial 3:00 or radial 1:30 α angle > 50.5° or 60°, respectively [47, 51, 60] (Fig. 1).

The femoral neck-shaft angle was measured for each hip (Fig. 1) using a DICOM viewer (Onis 2.4; DigitalCore, Tokyo, Japan) to confirm if the symptomatic group had a reduced neck angle [39-41]. For each of the three participant groups, the participant with the largest femoral neck-shaft angle and the participant with the smallest femoral neck-shaft angle were selected from the initial cohort (Table 1). Each participant's affected hip underwent subsequent MRI (MAGNETOM Symphony; Siemens

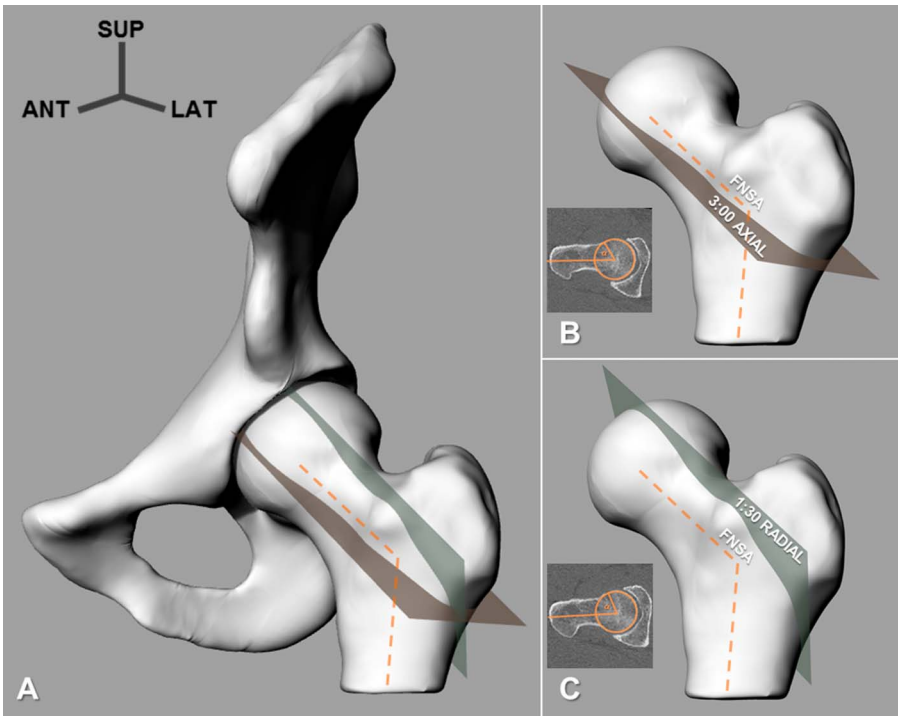

Fig. 1 A-C (**A**) The hip assembly is comprised of a segmented hemipelvis and proximal femur, indicating the α angle planes. Two planes were examined to determine if the femoral head had a cam deformity, where (**B**) the 3:00 axial plane is observed if α angle > 50.5° and (**C**) the 1:30 radial plane is observed if α angle > 60° (small insets depicts CT image). The femoral neck-shaft angle (FNSA) was determined to examine the effects of neck angles on each group's acetabular cartilage and subchondral bone stresses. SUP = superior; ANT = anterior; LAT = lateral.

Table 1. Summary of clinical assessments and measured anatomic parameters for each symptomatic, asymptomatic, and control participant with high (H) and low (L) femoral neck-shaft angle

Participant	Age (years)	BMI (kg/m^2)	HOOS Pain (%)	WOMAC Pain (%)	Axial 3:00 α angle (°)	Radial 1:30 α angle (°)	Femoral neck-shaft angle (°)
Symptomatic H	25	25	53	55	51	63	125
Symptomatic L	33	22	65	80	58	64	119
Asymptomatic H	28	27	100	100	52	66	134
Asymptomatic L	44	27	100	100	56	70	123
Control H	32	26	100	100	44	56	132
Control L	30	29	100	100	41	52	124

BMI = body mass index; HOOS = Hip Disability and Osteoarthritis Outcome Score.

Healthcare GmbH, Erlangen, Germany) using a field strength of 1.5 T (384 × 384 resolution, slice thickness of 3 mm) to determine cartilage thicknesses and labral contours. Participants did not indicate other hip pathologies, major lower limb injuries, or other musculoskeletal abnormalities. The study protocol was approved by the university and hospital research institute ethics boards and participants provided informed consent before the investigations.

Each participant's pelvis and femur bone models were manually segmented from CT data using segmentation software (3D-Doctor 4.0; Able Software Corp, Lexington, MA, USA). The MRI data were registered and centered on four control points of the target CT images, where the femoral head center and the acetabulum's deepest width and depth were landmarks for registration (Fig. 2A). The midpoints between the femoral and acetabular cartilages were located on each slice to determine cartilage thicknesses; and the femoral cartilage, acetabular cartilage, and labrum were manually segmented. All segmented models were then resurfaced to reduce geometric artifacts using computer-aided design software (SolidWorks; Dassault Systèmes, Concord, MA, USA) (Fig. 2B). To confirm the accuracy of the modeling procedure, anatomic hip parameters of the resurfaced models were measured using computer-aided design software and compared with the original CT data [43]. Soft tissues were modeled as smooth layers because none of the participants had osteoarthritis based on the imaging data.

Hip models were imported into finite element analysis software (ANSYS 12.1; ANSYS Inc, Canonsburg, PA, USA) and meshed with tetrahedral, SOLID187 elements. The meshes were then imported into a bone density mapping program (Bonemat Version 3.1; Istituto Ortopedico Rizzoli, Bologna, Italy). A linear density-elasticity relationship assigned subject-specific elastic moduli to individual elements based on the calibration phantom, resulting in heterogeneous, isotropic bone models [61] (Fig. 2C). Cartilage and labrum were modeled as Neo-Hookean, hyperelastic materials [24, 25] with constant hydrostatic pressure. Articular cartilage contacts were modeled with a frictional coefficient of 0.01 [63]. Element sizes for the bone and soft tissue models started at 3 and 2 mm, respectively, and were refined to ensure mesh sensitivity.

Each participant performed maximal squatting trials in the motion capture environment (Fig. 2D), similar to

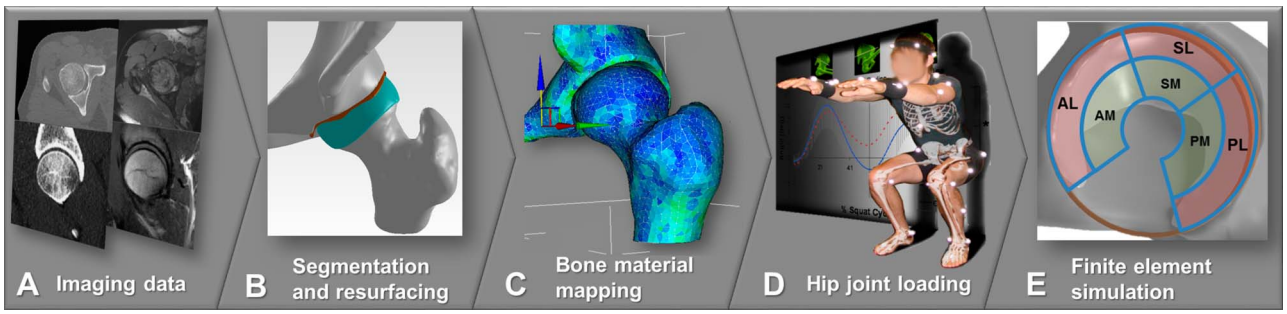

Fig. 2 A-E Summary of the process showing subject-specific input data used for finite element simulations. (**A**) CT and MRI data were used for modeling; (**B**) hip models were segmented and resurfaced; (**C**) subject-specific bone material properties were mapped to each bone model; (**D**) squat loads were applied; and (**E**) simulated to determine resultant hip stresses on the acetabular cartilage, labrum, and subchondral bone AL = anterolateral; AM = anteromedial; SL = superolateral; SM = superomedial; PL = posterolateral; PM = posteromedial.

previous squat protocols [32, 33, 39]. Three-dimensional kinematics were recorded using 10 infrared motion capture cameras (MX-13; Vicon, Oxford, UK) and retroreflective markers attached onto each participant's anatomic landmarks. The radiopaque pelvis markers were replaced with retroreflective markers and the motion trajectories were filtered using motion analysis software (Woltring, mean square error = 15 mm^2; Nexus 1.8.5; Vicon, Oxford, UK). Ground reaction forces were captured using two forceplates (FP4060-08; Bertec, Columbus, OH, USA) and filtered using numeric computational software (zero-lag, fourth-order Butterworth, cutoff frequency 6 Hz; MATLAB R2014a; MathWorks, Natick, MA, USA).

Hip contact forces were estimated using a musculoskeletal modeling program (OpenSim 3.1; SimTK, Stanford University, Palo Alto, CA, USA). The torso and lower limb segments modeled the hips and lumbar as ball-and-socket joints, which contributed to 23 degrees of freedom and 92 musculotendon actuators [13]. Muscle forces were determined using static optimization [37, 38] and the resultant three-dimensional hip contact forces were expressed in the pelvic reference system [65].

Because each participant had a different squat depth and pelvic ROM, a common quasistatic loading scenario was simulated to examine the midsquat condition at 90° of hip flexion (near 50% of leg length). In each finite element simulation, the hip contact forces were applied at the femoral head and boundary conditions were fixed at the pubis symphysis, iliac crest, and sacroiliac joint. Because cartilage is mostly under shear stress, which could indicate risks leading to cartilage failure and across the cartilage-bone interface [3, 49], maximum shear stresses were examined on each participant's acetabular cartilage, labrum, and subchondral bone to examine adverse loading conditions (Fig. 2E).

The femur was oriented according to the squatting position and the sectioned plane of the proximal diaphysis was fixed to permit translation in the direction of loading [25, 44] (Fig. 3). With two models per group (one representing the highest femoral neck-shaft angle and one representing the lowest), a full statistical analysis was not conducted because there was no statistical power. The range of the two values (maximum and minimum) that represents the resultant magnitudes from the models with the highest and lowest femoral neck-shaft angles are reported. A flowchart from subject-specific input data to resultant hip stresses is summarized (Appendix, Supplemental Digital Content 1, http://links.lww.com/CORR/A103).

Results

Both symptomatic and asymptomatic groups had higher cartilage stresses compared with the control subjects. The

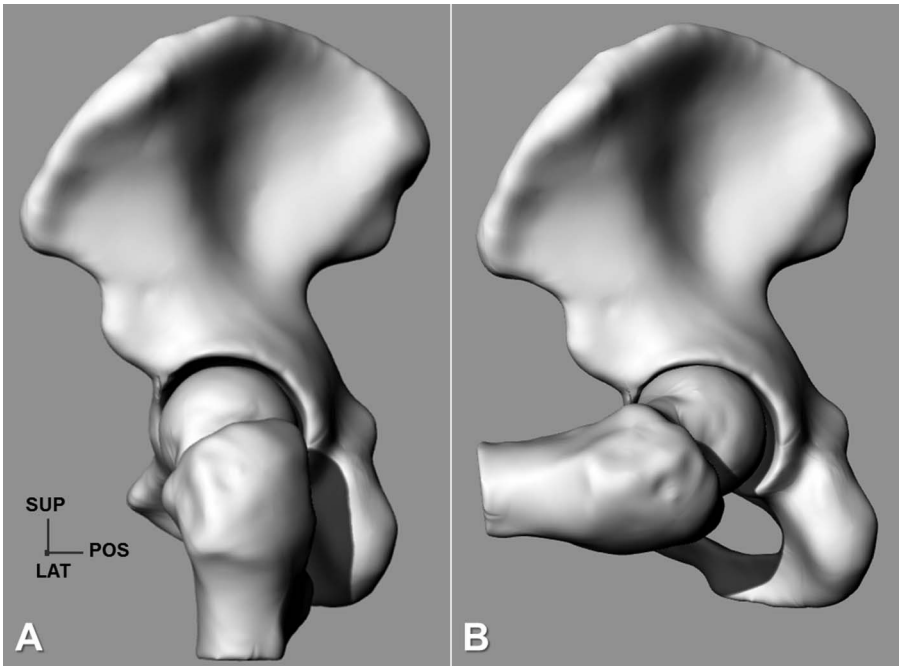

Fig. 3 A-B Sagittal view of the hip assembly during the neutral position (**A**) and the examined squatting position (**B**) is shown. Femur and pelvis models were oriented according to the kinematics at a midsquat condition of 90° hip flexion near 50% of leg height. SUP = superior; POS = posterior; LAT = lateral.

symptomatic participant with low femoral neck-shaft angle (119°) showed multiple peak stresses on the anterosuperior cartilage (absolute maximum peak = 10.4 MPa) with multiple stress concentrations in the posterior quadrant (Fig. 4). The symptomatic participant with a higher femoral neck-shaft angle (125°) had a much lower peak stress at the anterolateral cartilage (absolute maximum peak = 7.2 MPa) with a prominent secondary posteroinferior stress concentration. Both asymptomatic participants had anterolateral peak cartilage stresses with the lower femoral neck-shaft angle (123°) indicating a marginally higher peak stress (absolute maximum peak = 7.5 MPa) compared with the higher femoral neck-shaft angle (134°, absolute maximum peak = 6.9 MPa). Although there were no substantial differences in stress magnitudes between control subjects (peaks = 5.9, 6.2 MPa), the participant with high femoral neck-shaft angle visually showed more evenly distributed stresses (Fig. 4).

For both cam deformity (symptomatic and asymptomatic) groups, peak subchondral bone stresses were substantially higher than their corresponding cartilage stresses, whereas for the control group, there were marginal differences between peak cartilage and subchondral bone stresses (Fig. 5). Differences in femoral neck-shaft angle influenced both cam deformity groups. The symptomatic participant with low femoral neck-shaft angle (119°) had the highest stress in the anterosuperior region (absolute maximum peak = 15.8 MPa), whereas the higher femoral neck-shaft angle (125°) resulted in a lower magnitude stress concentration (absolute maximum peak = 14.1 MPa). Both symptomatic participants also revealed elevated secondary posterior stresses, perhaps as a result of contrecoup levering. The asymptomatic participants showed elevated anterolateral stresses; however, the participant with low femoral neck-shaft angle (123°) demonstrated elevated anterosuperior stress on the acetabular rim (peak = 13.0 MPa), whereas the asymptomatic participant with high femoral neck-shaft angle (134°) showed slightly lower stress (peak = 10.9 MPa). Both control participants experienced lower, well-distributed stresses (peaks = 6.4, 6.5 MPa; Fig. 6).

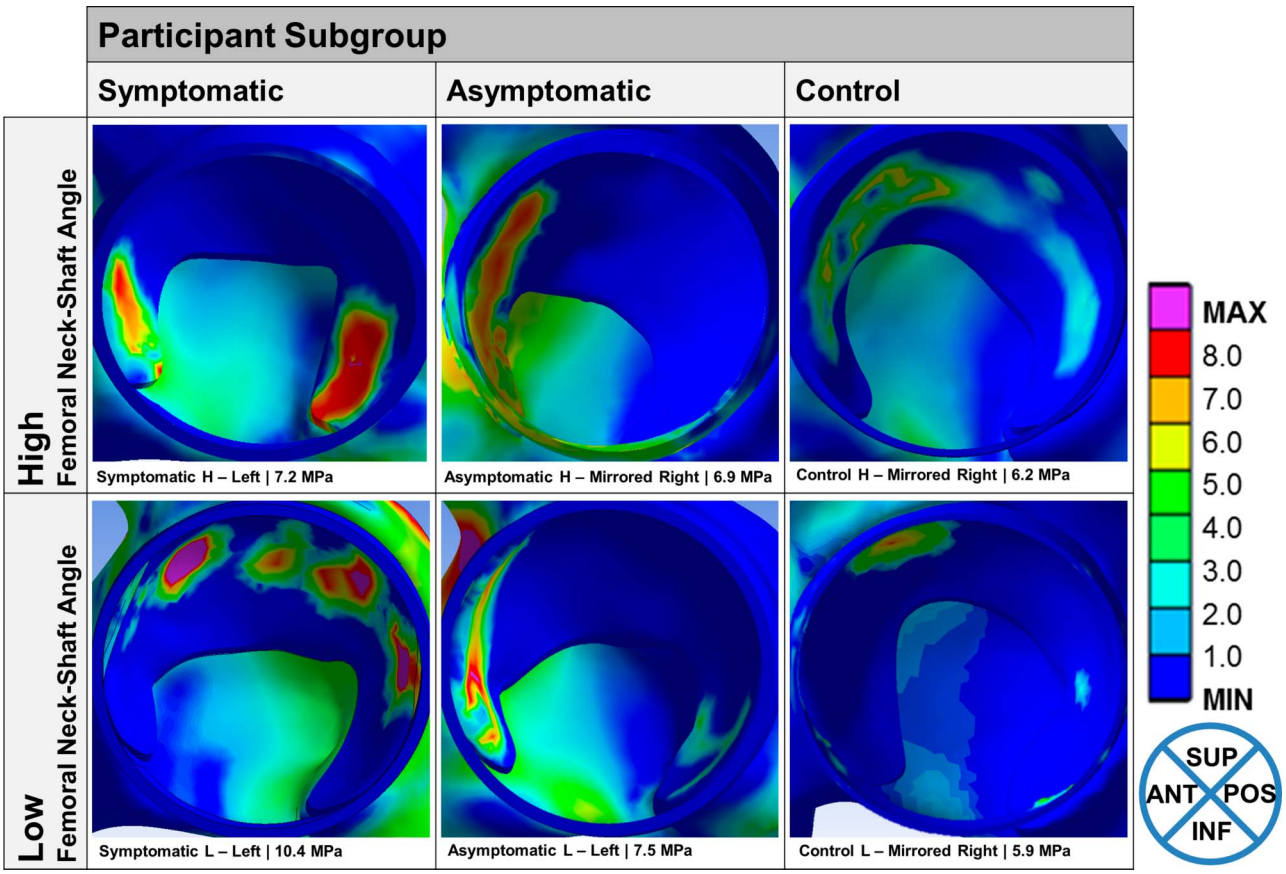

Fig. 4 Sagittal view of the acetabular cartilage and labrum showing the maximum shear stress distributions for each symptomatic, asymptomatic, and control participant with the highest (H; top row) and lowest (L; bottom row) femoral neck-shaft angle. The reference locations are denoted by anterior (ANT), posterior (POS), superior (SUP), and inferior (INF).

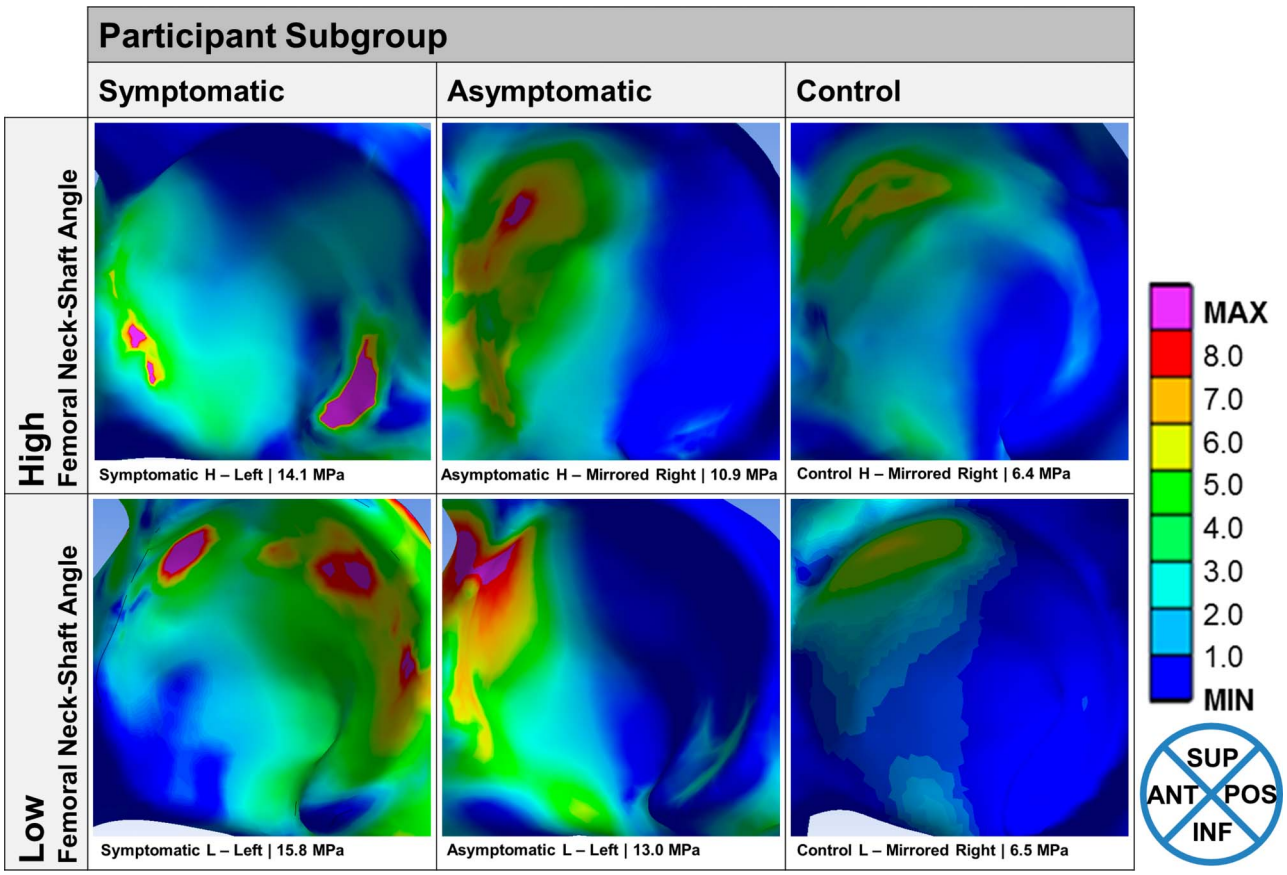

Fig. 5 Sagittal view of the acetabular subchondral bone showing the maximum shear stress distributions for each symptomatic, asymptomatic, and control participant with the highest (H; top row) and lowest (L; bottom row) femoral neck-shaft angle. The reference locations are denoted by anterior (ANT), posterior (POS), superior (SUP), and inferior (INF).

Discussion

Although individuals with a cam deformity and a smaller femoral neck angle may be more predisposed to symptoms of FAI [4, 39, 40, 52], it was unclear how these parameters (cam deformity and neck angle) affected impingement during hip loading. Finite element methods have shown utility in the simulation of cam FAI, indicating elevated hip stresses at extremes of motion [11, 12, 23, 27, 46]; however, there was a lack of subject specificity and a clinically defined asymptomatic population was not examined [42]. In this study we implemented subject-specific hip geometries, bone material properties, and hip loading data and observed that individuals with a cam deformity and a lower femoral neck-shaft angle were subjected to elevated subchondral bone stresses, which would increase the risks of early clinical signs and symptoms associated with FAI.

There are limitations of our study to consider and address for future research. First, our sampling was limited to extremes of femoral neck-shaft angles with only males included. Although cam deformity is more prevalent in the younger, male population, the small sample size and selection protocol do not account for the larger spectrum of anatomic variability to represent populations with more diverse morphologies [16, 22]. A larger sample size with female participants would improve the robustness to correlate impingement severities with associated anatomic parameters as well as permit the examination of other variables such as BMI and activity level. Second, hip contact forces were determined from static optimization as opposed to instrumented prostheses and thus were marginally higher. Differences in age, activity level, BMI, and hip pathology should be considered when comparing hip contact forces from instrumented prostheses [7]. Third, knowing that muscle loads contribute considerably to bone remodeling [8, 14] and capsular ligaments play a vital role in functional stability [21, 29, 64], it would be imperative to further examine the effects of the surrounding tissues on changes in hip contact forces in future work [9, 36].

Both cam deformity groups had slightly higher acetabular cartilage stresses compared with the control group; however, the individuals with a cam deformity and low

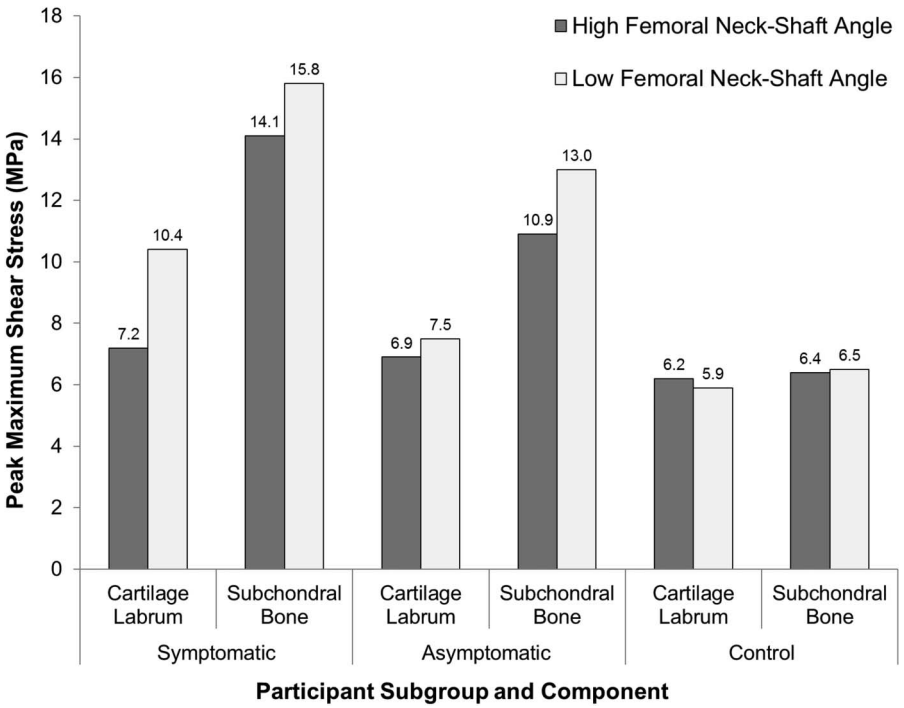

Fig. 6 Peak maximum shear stress on the acetabular cartilage-labrum and subchondral bone for each symptomatic, asymptomatic, and control participant with the highest and lowest femoral neck-shaft angle is shown.

femoral neck-shaft angle had substantially high cartilage stresses. Although previous finite element simulations were preliminary explorations of hip stresses resulting from cam FAI, none of the studies considered subject-specific loading characteristics or bone material properties or the effects of femoral neck-shaft angles to adequately characterize subgroups [42]. Previous studies also implemented either instrumented prosthesis loads or intersegmental reaction forces (from inverse dynamics) as opposed to hip contact forces (from static optimization and musculoskeletal modeling). Although an indirect comparison of stress parameters, our cam deformity groups' peak cartilage stresses were similar to Chegini and associates' [11] large range of contact pressures (3.67–12.84 MPa) and von Mises stresses (9.7–27.2 MPa) for cam deformities. However, they reconstructed an idealized ball-and-socket model, parameterized to several cam and acetabular coverage morphologies, and applied instrumented prosthesis forces for a stand-to-sit activity. Jorge and associates' [27] cam-type model also reported elevated peak contact pressures and von Mises stresses in the anterosuperior cartilage (11.6 and 14.4 MPa, respectively) and labrum (16.4 and 14.7 MPa, respectively) during deep flexion. Their study was limited to one male subject with a severe cam deformity (age, 27 years; α angle = 98°) matched with one female control subject (age, 50 years; α angle = 48°). In another recent finite element study, Sánchez Egea and associates [56] parameterized femoral neck-shaft (110°–130°), femoral torsion (0°–20°), and acetabular version angles (0°–20°), examining anatomic variations leading to hip cartilage stresses during quasistatic walking loads. Interestingly, their varus hip configuration (110°) also demonstrated higher stresses than their control model. However, their study parameterized one female model (age, 99 years; BMI, 23 kg/m^2) and did not account for any cam morphology. Although in our previous work we showed noticeable differences in hip kinematics between symptomatic and control participants [32, 33, 39], in this study, we selected a common squat depth (90° hip flexion, near 50% leg length) for all participants to compare hip stresses at the same amplitude of motion. Although the asymptomatic and control participants could squat slightly deeper than half of their leg length, this instance was selected because the symptomatic participants were very near the maximal squat depth. Anatomically, individuals with symptomatic FAI are more associated with anterior acetabular coverage and higher spinopelvic incidence angles [18, 41], and thus our symptomatic individuals squatted with their hips slightly abducted and externally rotated to perhaps avoid any discomfort and direct chondrolabral contact with the cam deformity.

The cam deformity groups' acetabular subchondral bone stresses were considerably higher than their associated cartilage stresses. Interestingly, the asymptomatic participant with the high femoral neck-shaft angle demonstrated cartilage stresses that were similar to the control group's cartilage stresses, but showed higher subchondral bone stresses compared with the control group. These findings align very closely with recent studies, in which acetabular subchondral bone was much denser in cam-type hips, regardless of clinical signs or symptoms [50, 59]. Both symptomatic and asymptomatic groups had stress concentrations that coincided with known areas of cartilage damage [6] and subchondral bone stiffening [59]. Both symptomatic participants had relatively low femoral neck-shaft angles compared with the asymptomatic and control groups. The asymptomatic participant with low femoral neck-shaft angle (123°) had similar peak stresses as the symptomatic participant with high femoral neck-shaft angle (125°). This further supports that neck angle parameters, combined with cam deformity parameters, are influential discriminants to predict early symptoms of cam FAI [39, 40] and perhaps can further associate varus hips with elevated adverse stresses leading to early labral tears and clinical signs and symptoms [4, 19, 53]. A varus hip may also be more susceptible to shear loading across the physeal growth plate [15, 48], which could predispose to slipped capital femoral epiphysis or cam FAI. In our earlier finite element study that compared hip stresses among symptomatic, asymptomatic, and control individuals during level walking [44], the symptomatic and asymptomatic participants with low femoral neck-shaft angles demonstrated higher peak cartilage stresses. The resultant higher stresses were not directly associated with higher hip contact loading, because the symptomatic participants (with denser subchondral bone) had lower estimated hip contact forces during squatting. Similar to our previous study on level walking [44, 45], this may have been the result of a compensatory mechanism to reduce hip contact loading. In an earlier finite element study by Fishkin and associates [15], a single male model with slipped capital femoral epiphysis was parameterized to various femoral versions, directional varus loading, and body weight loading parameters. The authors observed that varus loading conditions resulted in greater shear forces across the physis, which ultimately could increase the risk of morphologic changes. In recent in vivo ovine studies, Siebenrock and associates [57, 58] performed intertrochanteric osteotomies on eight healthy sheep hips. Although the ovine femoral heads did not indicate cam-like deformities, the femoral neck-shaft angles were surgically decreased to induce mechanical impingement. The surgical procedure clearly reproduced varus neck angles and resulted in chondrolabral degeneration [57], similar to progressive degeneration in human hips with FAI [58]. Ultimately, individuals with a cam deformity and decreased neck angle appear more likely to require surgical intervention to reduce adverse stresses and delay the degenerative process [5], whereas individuals with cam morphology and normal-to-higher femoral neck-shaft angles are at lesser risks of disease progression that potentially require surgical intervention [41, 45].

In conclusion, our study demonstrated that individuals with a cam deformity and lower femoral neck-shaft angles are subject to elevated subchondral bone stresses, which would increase the risks of early clinical signs and symptoms associated with FAI. Ultimately, the asymptomatic cam deformity can remain subclinical while predisposing to early subchondral bone stiffening and progressive joint degeneration. Future studies will expand the inputs for parametric finite element analyses, varying the size and location of the cam morphology, femoral neck-shaft angle, soft tissue envelope (for example, capsular ligaments, muscles) as well as the acetabular subchondral bone stiffness to better understand the contributions of individual anatomic parameters to the pathomechanisms of FAI.

Acknowledgments We thank Kawan Rakhra MD, FRCPC, from The Ottawa Hospital, for his help with CT readings; and Andrew Speirs PhD, from Carleton University, for his insights into bone material mapping.

References

1. Agricola R, Heijboer MP, Bierma-Zeinstra SM, Verhaar JA, Weinans H, Waarsing JH. Cam impingement causes osteoarthritis of the hip: a nationwide prospective cohort study (CHECK). *Ann Rheum Dis*. 2013;72:918-923.
2. Anwander H, Melkus G, Rakhra KS, Beaule PE. T1rho MRI detects cartilage damage in asymptomatic individuals with a cam deformity. *J Orthop Res*. 2016;34:1004-1009.
3. Ateshian GA, Henak CR, Weiss JA. Toward patient-specific articular contact mechanics. *J Biomech*. 2015;48:779-786.
4. Bardakos NV, Villar RN. Predictors of progression of osteoarthritis in femoroacetabular impingement: a radiological study with a minimum of ten years follow-up. *J Bone Joint Surg Br*. 2009;91:162-169.
5. Beaule PE, Speirs AD, Anwander H, Melkus G, Rakhra K, Frei H, Lamontagne M. Surgical correction of cam deformity in association with femoroacetabular impingement and its impact on the degenerative process within the hip joint. *J Bone Joint Surg Am*. 2017;99:1373-1381.
6. Beck M, Kalhor M, Leunig M, Ganz R. Hip morphology influences the pattern of damage to the acetabular cartilage: femoroacetabular impingement as a cause of early osteoarthritis of the hip. *J Bone Joint Surg Br*. 2005;87:1012-1018.
7. Bergmann G, Graichen F, Rohlmann A. Hip joint loading during walking and running, measured in two patients. *J Biomech*. 1993;26:969-990.
8. Bitsakos C, Kerner J, Fisher I, Amis AA. The effect of muscle loading on the simulation of bone remodelling in the proximal femur. *J Biomech*. 2005;38:133-139.
9. Bolia I, Chahla J, Locks R, Briggs K, Philippon MJ. Microinstability of the hip: a previously unrecognized pathology. *Muscles Ligaments Tendons J*. 2016;6:354-360.
10. Chakraverty JK, Sullivan C, Gan C, Narayanaswamy S, Kamath S. Cam and pincer femoroacetabular impingement: CT findings

of features resembling femoroacetabular impingement in a young population without symptoms. *AJR Am J Roentgenol*. 2013;200: 389-395.
11. Chegini S, Beck M, Ferguson SJ. The effects of impingement and dysplasia on stress distributions in the hip joint during sitting and walking: a finite element analysis. *J Orthop Res*. 2009;27: 195-201.
12. Cooper RJ, Williams S, Mengoni M, Jones AC. Patient-specific parameterised cam geometry in finite element models of femoroacetabular impingement of the hip. *Clin Biomech (Bristol, Avon)*. 2018;54:62-70.
13. Delp SL, Loan JP, Hoy MG, Zajac FE, Topp EL, Rosen JM. An interactive graphics-based model of the lower extremity to study orthopaedic surgical procedures. *IEEE Trans Biomed Eng*. 1990; 37:757-767.
14. Fernandez J, Sartori M, Lloyd D, Munro J, Shim V. Bone remodelling in the natural acetabulum is influenced by muscle force-induced bone stress. *Int J Numer Method Biomed Eng*. 2014;30:28-41.
15. Fishkin Z, Armstrong DG, Shah H, Patra A, Mihalko WM. Proximal femoral physis shear in slipped capital femoral epiphysis–a finite element study. *J Pediatr Orthop*. 2006;26:291-294.
16. Ganz R, Leunig M, Leunig-Ganz K, Harris WH. The etiology of osteoarthritis of the hip: an integrated mechanical concept. *Clin Orthop Relat Res*. 2008;466:264-272.
17. Ganz R, Parvizi J, Beck M, Leunig M, Notzli H, Siebenrock KA. Femoroacetabular impingement: a cause for osteoarthritis of the hip. *Clin Orthop Relat Res*. 2003;417:112-120.
18. Grammatopoulos G, Speirs AD, Ng KCG, Rivière C, Rakhra KS, Lamontagne M, Beaulé PE. The acetabular and spino-pelvic morphologies are different in subjects with symptomatic cam femoro-acetabular impingement. *J Orthop Res*. 2018;36: 1840-1848.
19. Guevara CJ, Pietrobon R, Carothers JT, Olson SA, Vail TP. Comprehensive morphologic evaluation of the hip in patients with symptomatic labral tear. *Clin Orthop Relat Res*. 2006;453: 277-285.
20. Hack K, Di Primio G, Rakhra K, Beaule PE. Prevalence of cam-type femoroacetabular impingement morphology in asymptomatic volunteers. *J Bone Joint Surg Am*. 2010;92:2436-2444.
21. Han S, Alexander JW, Thomas VS, Choi J, Harris JD, Doherty DB, Jeffers JRT, Noble PC. Does capsular laxity lead to microinstability of the native hip? *Am J Sports Med*. 2018;46:1315-1323.
22. Hartofilakidis G, Bardakos NV, Babis GC, Georgiades G. An examination of the association between different morphotypes of femoroacetabular impingement in asymptomatic subjects and the development of osteoarthritis of the hip. *J Bone Joint Surg Br*. 2011;93:580-586.
23. Hellwig FL, Tong J, Hussell JG. Hip joint degeneration due to cam impingement: a finite element analysis. *Comput Methods Biomech Biomed Engin*. 2016;19:41-48.
24. Henak CR, Abraham CL, Anderson AE, Maas SA, Ellis BJ, Peters CL, Weiss JA. Patient-specific analysis of cartilage and labrum mechanics in human hips with acetabular dysplasia. *Osteoarthritis Cartilage*. 2014;22:210-217.
25. Henak CR, Ellis BJ, Harris MD, Anderson AE, Peters CL, Weiss JA. Role of the acetabular labrum in load support across the hip joint. *J Biomech*. 2011;44:2201-2206.
26. Hunt MA, Guenther JR, Gilbart MK. Kinematic and kinetic differences during walking in patients with and without symptomatic femoroacetabular impingement. *Clin Biomech (Bristol, Avon)*. 2013;28:519-523.
27. Jorge JP, Simoes FM, Pires EB, Rego PA, Tavares DG, Lopes DS, Gaspar A. Finite element simulations of a hip joint with femoroacetabular impingement. *Comput Methods Biomech Biomed Engin*. 2014;17:1275-1284.
28. Jung KA, Restrepo C, Hellman M, AbdelSalam H, Morrison W, Parvizi J. The prevalence of cam-type femoroacetabular deformity in asymptomatic adults. *J Bone Joint Surg Br*. 2011;93: 1303-1307.
29. Kalisvaart MM, Safran MR. Microinstability of the hip-it does exist: etiology, diagnosis and treatment. *J Hip Preserv Surg*. 2015;2:123-135.
30. Kennedy MJ, Lamontagne M, Beaule PE. Femoroacetabular impingement alters hip and pelvic biomechanics during gait walking biomechanics of FAI. *Gait Posture*. 2009;30:41-44.
31. Khanna V, Caragianis A, Diprimio G, Rakhra K, Beaule PE. Incidence of hip pain in a prospective cohort of asymptomatic volunteers: is the cam deformity a risk factor for hip pain? *Am J Sports Med*. 2014;42:793-797.
32. Lamontagne M, Brisson N, Kennedy MJ, Beaule PE. Preoperative and postoperative lower-extremity joint and pelvic kinematics during maximal squatting of patients with cam femoro-acetabular impingement. *J Bone Joint Surg Am*. 2011; 93(Suppl 2):40-45.
33. Lamontagne M, Kennedy MJ, Beaule PE. The effect of cam FAI on hip and pelvic motion during maximum squat. *Clin Orthop Relat Res*. 2009;467:645-650.
34. Mantovani G, Ng KC, Lamontagne M. Regression models to predict hip joint centers in pathological hip population. *Gait Posture*. 2016;44:48-54.
35. McGuffin WS, Melkus G, Rakhra KS, Beaule PE. Is the contralateral hip at risk in patients with unilateral symptomatic cam femoroacetabular impingement? A quantitative T1rho MRI study. *Osteoarthritis Cartilage*. 2015;23:1337-1342.
36. Mitchell RJ, Gerrie BJ, McCulloch PC, Murphy AJ, Varner KE, Lintner DM, Harris JD. Radiographic evidence of hip microinstability in elite ballet. *Arthroscopy*. 2016;32: 1038-1044.e1031.
37. Modenese L, Gopalakrishnan A, Phillips AT. Application of a falsification strategy to a musculoskeletal model of the lower limb and accuracy of the predicted hip contact force vector. *J Biomech*. 2013;46:1193-1200.
38. Modenese L, Phillips ATM. Prediction of hip contact forces and muscle activations during walking at different speeds. *Multibody Syst Dyn*. 2012;28:157-168.
39. Ng KCG, Lamontagne M, Adamczyk AP, Rakhra KS, Beaule PE. Patient-specific anatomical and functional parameters provide new insights into the pathomechanism of cam FAI. *Clin Orthop Relat Res*. 2015;473:1289-1296.
40. Ng KCG, Lamontagne M, Beaule PE. Differences in anatomical parameters between the affected and unaffected hip in patients with bilateral cam-type deformities. *Clin Biomech (Bristol, Avon)*. 2016;33:13-19.
41. Ng KCG, Lamontagne M, Jeffers JRT, Grammatopoulos G, Beaule PE. Anatomic predictors of sagittal hip and pelvic motions in patients with a cam deformity. *Am J Sports Med*. 2018;46:1331-1342.
42. Ng KCG, Lamontagne M, Labrosse MR, Beaule PE. Hip joint stresses due to cam-type femoroacetabular impingement: a systematic review of finite element simulations. *PLoS One*. 2016;11: e0147813.
43. Ng KCG, Lamontagne M, Labrosse MR, Beaulé PE. Comparison of anatomical parameters of cam femoroacetabular impingement to evaluate hip joint models segmented from CT data. *Comput Methods Biomech Biomed Engin*. 2016;6:293-302.
44. Ng KCG, Mantovani G, Lamontagne M, Labrosse MR, Beaule PE. Increased hip stresses resulting from a cam deformity and

decreased femoral neck-shaft angle during level walking. *Clin Orthop Relat Res*. 2017;475:998-1008.
45. Ng KCG, Mantovani G, Modenese L, Beaule PE, Lamontagne M. Altered walking and muscle patterns reduce hip contact forces in individuals with symptomatic cam femoroacetabular impingement. *Am J Sports Med*. 2018;46:2615-2623.
46. Ng KCG, Rouhi G, Lamontagne M, Beaule PE. Finite element analysis examining the effects of cam FAI on hip joint mechanical loading using subject-specific geometries during standing and maximum squat. *HSS J*. 2012;8:206-212.
47. Notzli HP, Wyss TF, Stoecklin CH, Schmid MR, Treiber K, Hodler J. The contour of the femoral head-neck junction as a predictor for the risk of anterior impingement. *J Bone Joint Surg Br*. 2002;84:556-560.
48. Pritchett JW, Perdue KD. Mechanical factors in slipped capital femoral epiphysis. *J Pediatr Orthop*. 1988;8:385-388.
49. Radin EL, Burr DB, Caterson B, Fyhrie D, Brown TD, Boyd RD. Mechanical determinants of osteoarthrosis. *Semin Arthritis Rheum*. 1991;21:12-21.
50. Radin EL, Paul IL, Tolkoff MJ. Subchondral bone changes in patients with early degenerative joint disease. *Arthritis Rheum*. 1970;13:400-405.
51. Rakhra KS, Sheikh AM, Allen D, Beaule PE. Comparison of MRI alpha angle measurement planes in femoroacetabular impingement. *Clin Orthop Relat Res*. 2009;467:660-665.
52. Ranawat AS, Schulz B, Baumbach SF, Meftah M, Ganz R, Leunig M. Radiographic predictors of hip pain in femoroacetabular impingement. *HSS J*. 2011;7:115-119.
53. Redmond JM, Gupta A, Hammarstedt JE, Stake CE, Dunne KF, Domb BG. Labral injury: radiographic predictors at the time of hip arthroscopy. *Arthroscopy*. 2015;31:51-56.
54. Rylander J, Shu B, Favre J, Safran M, Andriacchi T. Functional testing provides unique insights into the pathomechanics of femoroacetabular impingement and an objective basis for evaluating treatment outcome. *J Orthop Res*. 2013;31:1461-1468.
55. Rylander JH, Shu B, Andriacchi TP, Safran MR. Preoperative and postoperative sagittal plane hip kinematics in patients with femoroacetabular impingement during level walking. *Am J Sports Med*. 2011;39(Suppl):36S-42S.
56. Sánchez Egea AJ, Valera M, Parraga Quiroga JM, Proubasta I, Noailly J, Lacroix D. Impact of hip anatomical variations on the cartilage stress: a finite element analysis towards the biomechanical exploration of the factors that may explain primary hip arthritis in morphologically normal subjects. *Clin Biomech (Bristol, Avon)*. 2014;29:444-450.
57. Siebenrock KA, Fiechter R, Tannast M, Mamisch TC, von Rechenberg B. Experimentally induced cam impingement in the sheep hip. *J Orthop Res*. 2013;31:580-587.
58. Siebenrock KA, Kienle KP, Steppacher SD, Tannast M, Mamisch TC, von Rechenberg B. Biochemical MRI predicts hip osteoarthritis in an experimental ovine femoroacetabular impingement model. *Clin Orthop Relat Res*. 2015;473:1318-1324.
59. Speirs AD, Beaule PE, Rakhra KS, Schweitzer ME, Frei H. Increased acetabular subchondral bone density is associated with cam-type femoroacetabular impingement. *Osteoarthritis Cartilage*. 2013;21:551-558.
60. Sutter R, Dietrich TJ, Zingg PO, Pfirrmann CW. How useful is the alpha angle for discriminating between symptomatic patients with cam-type femoroacetabular impingement and asymptomatic volunteers? *Radiology*. 2012;264:514-521.
61. Taddei F, Cristofolini L, Martelli S, Gill HS, Viceconti M. Subject-specific finite element models of long bones: an in vitro evaluation of the overall accuracy. *J Biomech*. 2006;39:2457-2467.
62. Tannast M, Siebenrock KA, Anderson SE. Femoroacetabular impingement: radiographic diagnosis–what the radiologist should know. *AJR Am J Roentgenol*. 2007;188:1540-1552.
63. Unsworth A, Dowson D, Wright V. The frictional behavior of human synovial joints—Part I: natural joints. *Journal of Lubrication Technology*. 1975;97:369-376.
64. van Arkel RJ, Amis AA, Jeffers JR. The envelope of passive motion allowed by the capsular ligaments of the hip. *J Biomech*. 2015;48:3803-3809.
65. Wu G, Siegler S, Allard P, Kirtley C, Leardini A, Rosenbaum D, Whittle M, D'Lima DD, Cristofolini L, Witte H, Schmid O, Stokes I; Standardization and Terminology Committee of the International Society of Biomechanics. ISB recommendation on definitions of joint coordinate system of various joints for the reporting of human joint motion–part I: ankle, hip, and spine. International Society of Biomechanics. *J Biomech*. 2002;35:543-548.